# Multiple Reference Optical Coherence Tomography (MR-OCT) System

Martin Leahy[1], Josh Hogan[2], Carol Wilson[2], Hrebesh Subhash[1], Roshan Dsouza[1]

[1]Tissue Optics and Microcirculation Imaging Group, School of Physics, National University of Ireland, Galway, Ireland
[2]Compact Imaging, Inc., 897 Independence Ave., Suite 5B, Mountain View, CA 94043 USA

## ABSTRACT

We describe a multiple reference OCT (MR-OCT) system which is radically different from existing optical coherence tomography (OCT) systems. Complete scans of a target from surface to depth are accomplished by simultaneously acquiring the scan in multiple segments using a virtually solid state design that is inherently miniature, robust and low cost; in short, ideal for use in applications characterized by high volumes, difficult operating environments and constrained acquisition and operating budgets.

## 1. INTRODUCTION

In conventional time domain TD-OCT systems depth scanning is achieved by modifying the relative optical path length of the reference path and the probe path. The relative path length is modified by such techniques as electromechanical based technologies, such as galvanometers **[1, 2]** or moving coil actuators, rapid scanning optical delay lines **[3,4,5]** and rotating polygons **[6]**. All of these techniques involve moving parts that have to move a substantial distance, which have limited scan speeds and present significant alignment and associated signal to noise ratio (SNR) related problems. Motion occurring within the duration of scan can cause significant problems in correct signal detection. If motion occurs within a scan duration, motion related artifacts will be indistinguishable from real signal information in the detected signal, leading to an inaccurate measurement. Long physical scans, for larger signal differentiation or locating reference areas, increase the severity of motion artifacts. Problematic motion can also include variation of the orientation of the target surface (skin) where small variations can have significant effects on measured scattering intensities.

Non-moving part solutions, include acousto-optic scanning **[7],** can be high speed, however such solutions are costly, bulky and have significant thermal control and associated thermal SNR related problems. Optical fiber based OCT systems also use piezo electric fiber stretchers. These, however, have polarization rotation related signal to noise ratio problems and also are physically bulky, are expensive, require relatively high voltage control systems and also have the motion related issues. These aspects cause conventional OCT systems to have significant undesirable SNR characteristics and present problems in practical implementations with sufficient accuracy, compactness and robustness at a price point for commercially viable and accurate imaging and analysis devices.

Fourier domain (FD) OCT systems are also currently available in two versions, swept source (SS-OCT) **[8]** and spectral domain (SD-OCT) **[9]**. SS-OCT uses an optical source consisting of a laser whose lasing wavelength is swept to achieve scanning. In an SD-OCT system, an optical spectrometer is used to separate the interferometric signal into individual wavelength to achieve the Fourier domain based depth information. To date, however, there is no low cost FD-OCT solution commercially available.

Therefore, there is an unmet need for commercially viable, low cost, compact, robust, non-invasive imaging and analysis technology and devices with sufficient accuracy, precision and repeatability to image or analyse targets or to measure analyte concentrations, and in particular to image and analyse human tissue.

## 1.1 Multiple reference optical coherence tomography (MR-OCT):

MR-OCT is similar to conventional TD-OCT, except a partial mirror is placed very close to the reference mirror (see Figure 1). The partial mirror causes the light to be reflected back and forth multiple times between the partial mirror and the reference mirror.

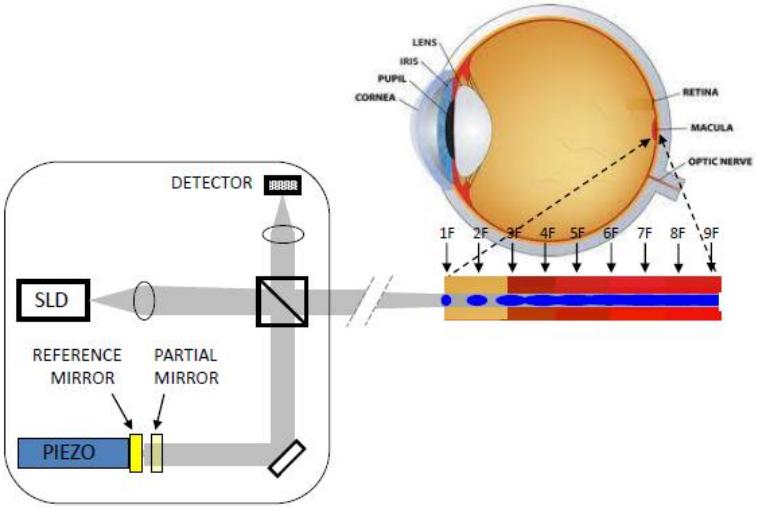


Figure 1: Schematic of MR-OCT system **[10,11]** (configured for retinal measurements)**.**

At each reflection, a small amount of light is transmitted through the partial mirror to the beam splitter and on to the detector to form reference light. The remaining portion of the light is reflected back to the reference mirror to form successive reflections. Each reflection between the partial and reference mirrors is delayed by the round trip time between the two mirrors. The resulting interference signals correspond to light backscattered from regions successively deeper within the target.

The center points of the interference or scan regions are separated by a distance equal to the distance between the partial mirror and the reference mirror. These scan region center points are indicated in Figure 1 by set of arrows pointing downward towards the target. The region from which backscattered light will generate an interference signal with the first reflection of the reference mirror (the dot under the arrow labeled "1F" in Figure 1) is same as in a conventional TD-OCT system. The region from which backscattered light will generate an interference signal with the reference light reflected two times is labeled "2F" in Figure 1. Because of the double pass, this second scan covers a region that is two times larger than the region covered by the first reflection. Likewise, the third scan region, generated from reference light reflected three times, covers a region that is three times larger than that of the first region and so on. These interference regions of continuously increasing size quickly begin to overlap (as indicated by the increasing size of the ovals in Figure 1). From the point that the scan regions begin to overlap, they provide the data for a continuous scan of the target.

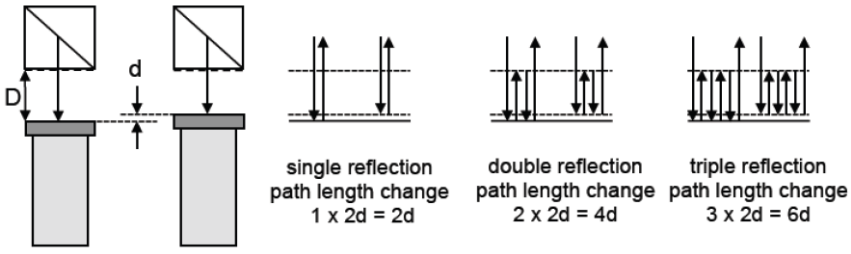


Figure 2: Schematic of multiple reflections at the reference arm.

Systematic increase in the path length change will correspond to systematic increase in the electronic frequency of the detected interference signals associated with the multiple references. For example, the path length change for the second order reference light is twice that of the first order reference light because of the double pass. And, since this path length change occurs in the same time duration for both orders of reflected light, the electronic frequency of the second order detected interference signal will be twice that of the first order. The frequencies of the different interference signals are all determined by the single pass piezo scan multiplied by the number of the reflection. This is illustrated in Figure 2.

Because of the systematic increase in the frequency of the interference signals associated with the increasing reflection orders, which corresponds to deeper and longer scan regions with the sample, it is possible to determine the particular profile of each scan region by separating out the interference signals using electronic filtering or digital signal processing techniques. This information from all the scan regions can be stitched together to form a continuous image. The deeper scan regions that overlap form a continuous scan with no gaps between the regions. The lower order (i.e. less deep) scans will not overlap and will have unscanned regions between them. Importantly, since some portions of higher order (i.e. deeper) regions are scanned by at least two overlapping scans, MR-OCT provides a mechanism for correlating scans to normalize and/or reduce noise in scans. In addition, the fact that multiple scans, covering a complete region, are acquired simultaneously improves the speed with which the complete region can be imaged or analysed, thus reducing sensitivity to motion artifacts.

## 2. MATERIALS AND METHODS

The experimental set up of an MR-OCT system is shown in Figure 3.

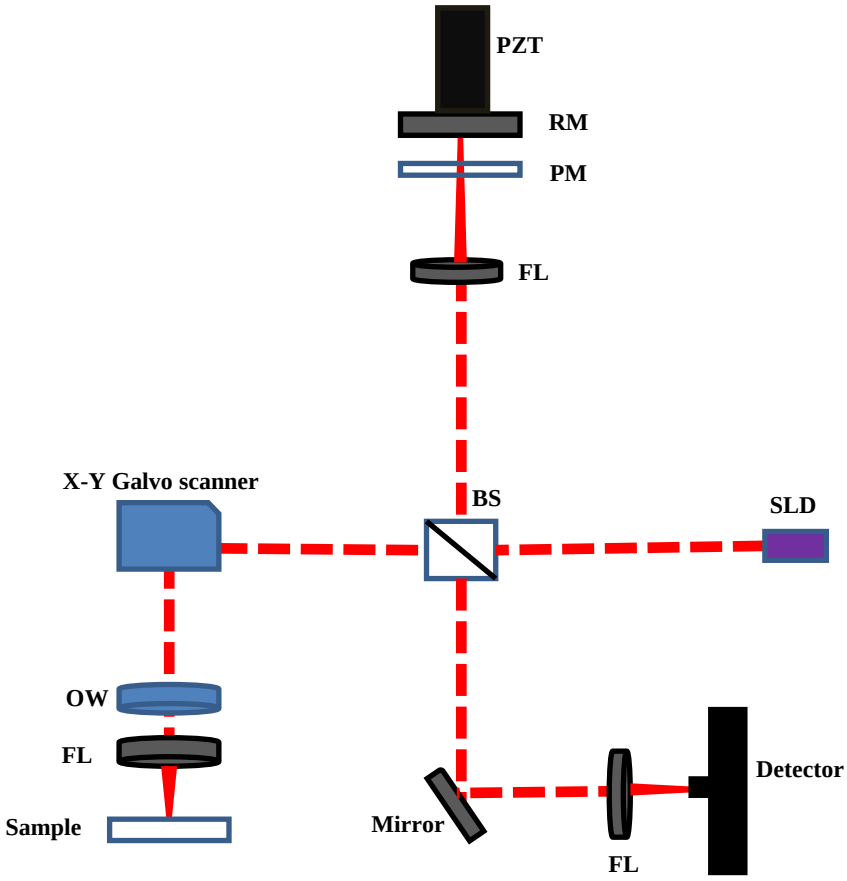


Figure 3: Experimental setup of MR-OCT (configured for tissue imaging). (SLD-Superluminescent Diode; BS-Beam Splitter; FL-Focusing Lens; PM-Partial Mirror; RM-Reference Mirror; PZT- Piezoelectric Transducer; OW-Optical Window)

The MR-OCT system uses a high power broadband superluminescent diode (DENSELIGHT, CS3159A) as the optical source, with a center wavelength of 1310 nm, spectral bandwidth of 83 nm, and an output power of 15 mW. The light emitted by the source is collimated using a collimating lens and is allowed to fall on a 50/50 beam splitter (Newport, 05BC17MB.3), which splits 50% of the power to the sample arm and the other 50% to the reference arm. The depth scanning is achieved by a piezoelectric transducer (PI Instruments, P-620.1CD) driven at a frequency of 50 Hz. A partial mirror is placed very close to the reference mirror (separation distance ~80 μm). The partial mirror causes the light to be reflected back and forth multiple times between the partial mirror and the reference mirror. The lateral scanning is achieved by an X-Y galvo scanner. Then light is focused into the sample using an objective lens (Thorlabs AC254050C) with a focal length of 50 mm and Numerical Aperture = 0.25. The light reflected back from both these arms will interfere at the surface of the photo detector (Newport, 2053FS) to produce the interference pattern.

## 3. RESULTS AND DISCUSSION

### 3.1 Relative intensity measurements:

There is a decrease in the intensity of the reference beam components corresponding to higher order multiple passes. The amount of this decrease in intensity depends on the partially reflecting element. Suppose the partial reflective element reflects 50% and transmits 50%. Then the reference beam component from the partially reflective element will have a relative intensity of approximately 50%; the reference beam component from a single pass will have a relative intensity of approximately 25%. Similarly, for double pass 12.5%, for triple pass 6.25% and so on. We simulated the reflection losses of various orders with respect to transmission and reflection of the partially reflecting element (Figure 4). A partially reflecting element with 90/10 (Transmission/Reflection) had a larger decay in intensity for higher orders, whereas a partially reflecting element with 10/90 (Transmission/Reflection) had a minimal decay in intensity.

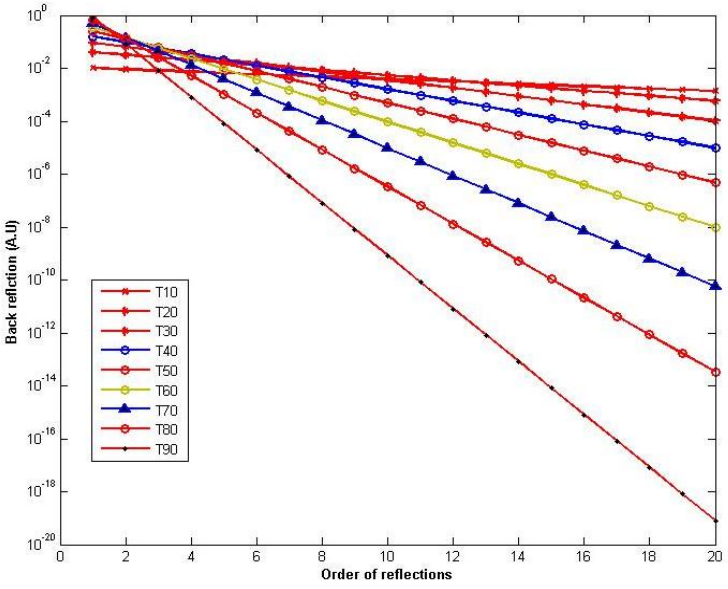


Figure 4: Log plot of relative intensity measurement for various orders.

Figure 5 depicts the signals resulting from multiple reflections. We did a simple experiment to prove the concept of multiple reflections by placing a mirror as a sample. Separation between the partial mirror and reference mirror was ~80 μm. The piezoelectric transducer (PZT) was driven at a frequency of 50 Hz, resulting in a scan range of 50 μm. According to the concept, for the second reflection the path length change is 100 μm, because of the double pass, and so on for higher orders. In Figure 5(C), the third scan region begins to overlap with the fourth scan region. In Figure 5(D), successively higher scan regions overlap.

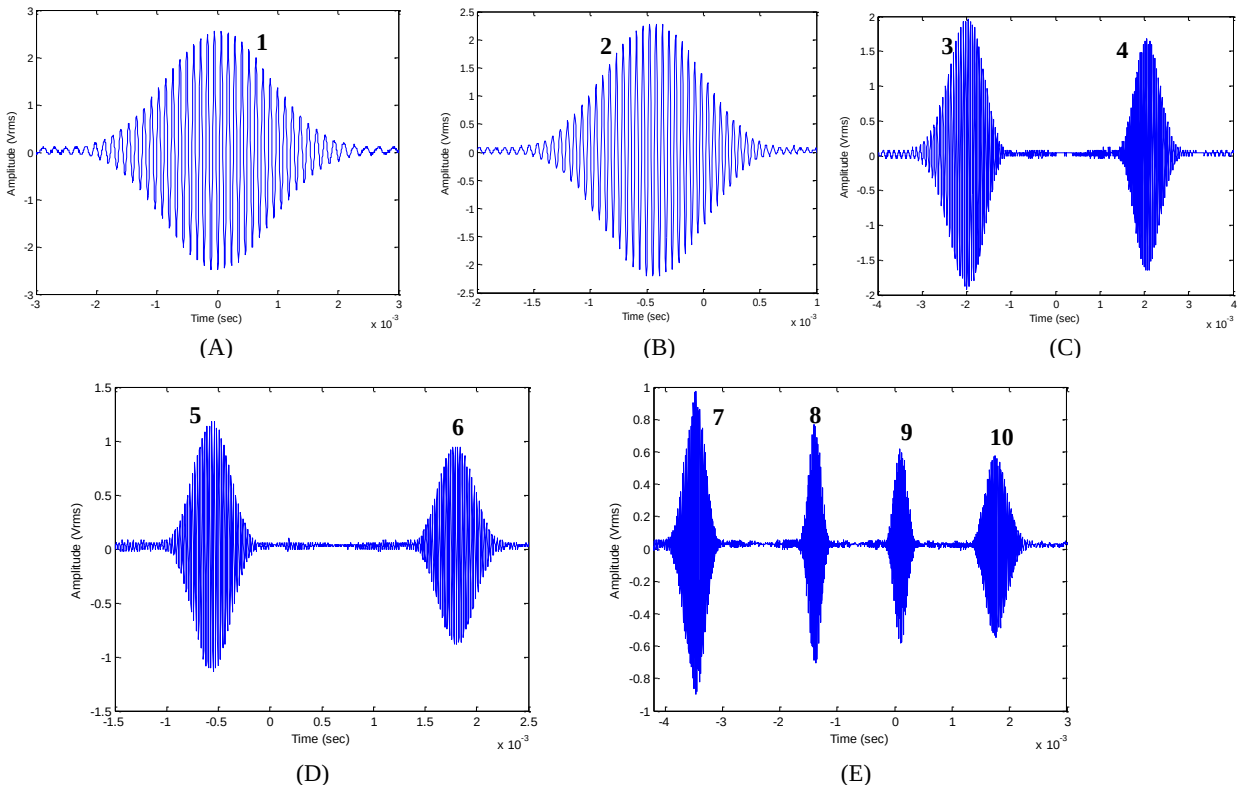


Figure 5: (A) 1st order reflection. (B) 2nd order reflection. (C) Overlap of 3rd and 4th order reflections. (D) Overlap of 5th and 6th order reflections. (E) Successively overlapping 7th – 10th order reflections.

Systematic increase in the path length change will correspond to systematic increase in the electronic frequency of the detected interference signals associated with the multiple references. Table 1 shows the measured and calculated electronic frequency of the MR-OCT system at each order.

| **Orders** | **1** | **2** | **3** | **4** | **5** | **6** | **7** | **8** | **9** | **10** |
|---|---|---|---|---|---|---|---|---|---|---|
| **Beat Frequency (kHz)** | **2.56** | **5.13** | **7.69** | **10.25** | **12.8** | **15.36** | **17.95** | **20.52** | **23.08** | **25.6** |
| **FFT (kHz)** | **2.9** | **5.2** | **7.6** | **10.4** | **12.8** | **15.6** | **18** | **20.4** | **23.2** | **25.04** |

Table 1: Electronic frequency of MR-OCT system at each order.

## 3.2 Sensitivity of MR-OCT system:

The sensitivity of the system was measured by using a mirror as a test object. During measurement the irradiation power on the sample surface was around 1.34 μW. Inserting an OD-3 (optical density-3) filter in the sample arm attenuates the signal light with a roundtrip attenuation of 60 dB. A variable attenuator filter was placed in the reference arm to prevent the detector from saturating. Reducing power in the reference arm will result in increasing SNR **[12].** Table 2 depicts the measured sensitivity of the MR-OCT system for each reflection.

| Orders | 1 | 2 | 3 | 4 | 5 |
|---|---|---|---|---|---|
| SNR (dB) | 93.54 | 92.02 | 91.93 | 91.88 | 90.98 |

Table 2: Measured SNR of MR-OCT system.

### 3.3 Non-linearity correction:

We need to linearize the PZT signal because we use a sine wave to drive the PZT, which is not linear with time. The data sampled at these intervals in time results in warping of the image. Here we use two different methods to correct (de-warp) the non-linearity of the signal: PZT position detection and zero crossing detection. In the PZT position detection approach, the PZT position output follows the actual position of the scanner very closely, thereby monitoring the effects of inertia and the characteristics of the feedback loop of the scanner.

Results are shown in Figure 6. Figure 6(A) depicts the uncorrected image. Figure 6(B) shows the corrected image using PZT method and Figure 6(C) shows the corrected image using zero crossing method. In order to compare between two methods, we took a surface plot of the corresponding image (left hand line over image). In Figure 6(E) the continuous line corresponds PZT method, whereas the dashed line corresponds zero crossing. With these results, we can clearly confirm both methods are accurate.

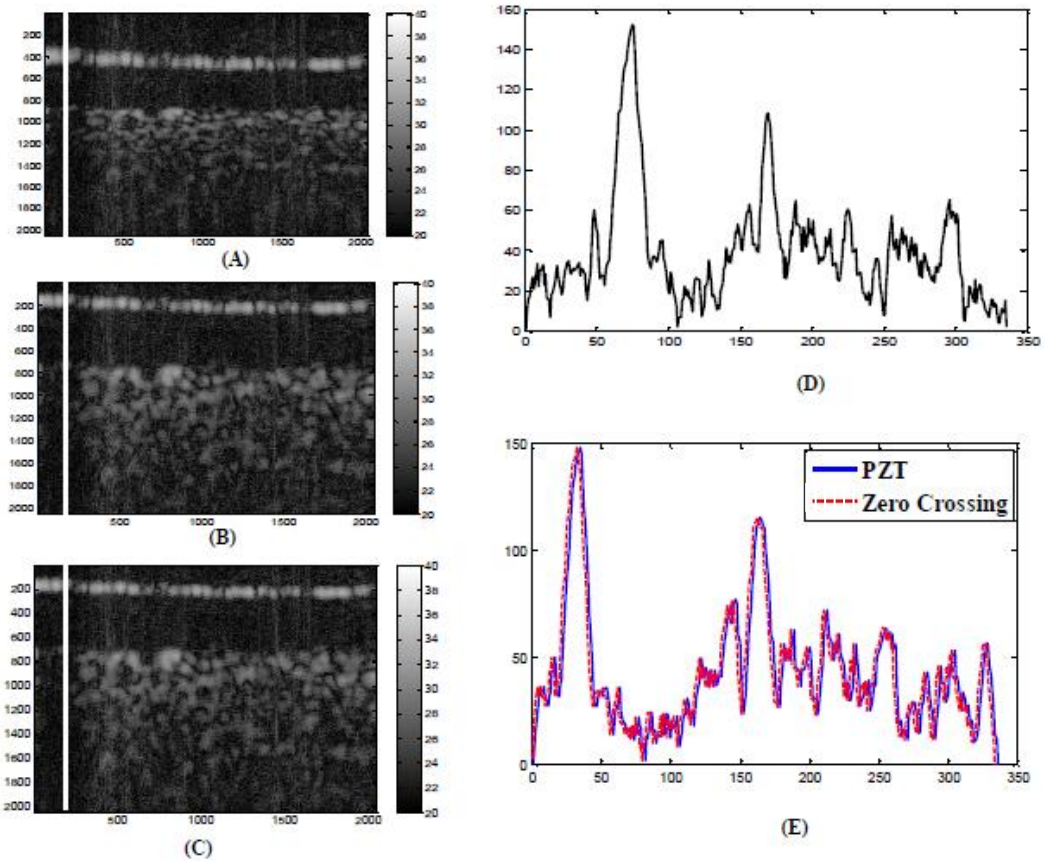


Figure 6: (A) Uncorrected image. (B) Corrected using PZT method. (C) Corrected using zero crossing method. (D) Surface plot profile of uncorrected image. (E) Surface plot profile of corrected image (PZT (continuous line) and zero crossing (dashed line)).

Figure 7(A) shows an MR-OCT image of normal white paper wrapped with transparent adhesive tape. In this image we can clearly differentiate the two layers (tape and paper). The depth is measured to be ~300 μm with a lateral span 1.5 mm. Figure 7(B) depicts an MR-OCT image of normal white paper wrapped with two layers of tape. The layers of tape can be easily differentiated in the image. These images were recorded using the using the 6$^{th}$ order reflection with a PZT scanning range of 50 μm.

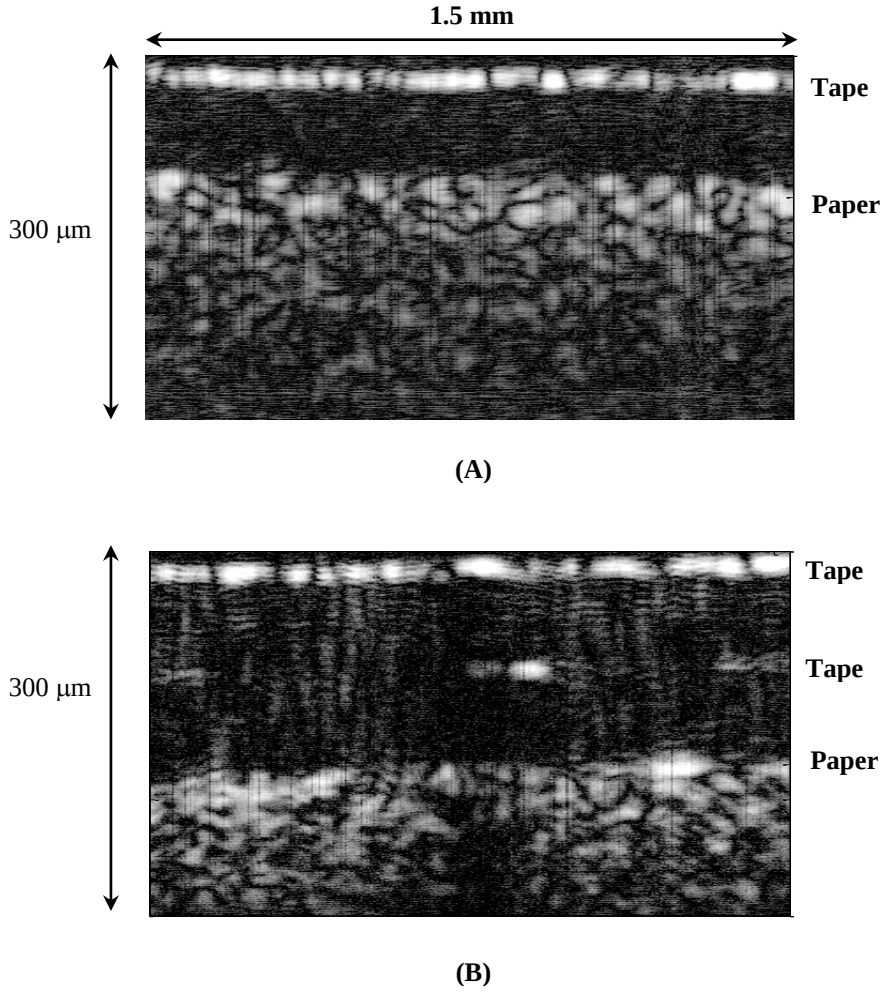


Figure 7: (A) MR-OCT image of tape-paper. (B) MR-OCT image of tape-tape-paper.

## 4. CONCLUSIONS

In summary, we have demonstrated the feasibility of the *MRO*™ multiple reference optical coherence tomography (MR-OCT) system invented at Compact Imaging, Inc., and we are now developing its capabilities as a new imaging modality in the OCT family. In an MR-OCT system, complete scans of a target from surface to depth are accomplished by simultaneously acquiring the scan in multiple segments using a virtually solid state design that is inherently miniature, robust and low cost; in short, ideal for use in applications characterized by high volumes. As a first follow-on step, we have confirmed that the SNR performance of MR-OCT is similar to that of conventional TD-OCT systems. The operation of the system was demonstrated using two example targets, clearly showing the ability to distinguish the

layered structure. The illustrated MR-OCT sensor could be implemented as a very small device (comparable in size and complexity to the optical pick up unit of a DVD player) at a small fraction of the cost of conventional OCT systems.

## REFERENCES


1. J. A. Izatt, M. D. Kulkarni, H.-W. Wang, K. Kobayashi, and M. V. Sivak Jr., "Optical Coherence Tomography and Microscopy in Gastrointestinal issues," IEEE J. Sel. Top. Quant. Elect **2**, 1017-1028 (1996).
2. E. A. Swanson, D. Huang, M. R. Hee, J. G. Fujimoto, C. P. Lin, and C. A. Puliafito, "High-speed optical coherence domain reflectometry," Opt. Lett. **17**, 151-153 (1992).
3. Andrew Rollins, Siavash Yazdanfar, Manish Kulkarni, Rujchai Ung-Arunyawee, and Joseph Izatt, "In vivo video rate optical coherence tomography," Opt. Express **3**, 219-229 (1998).
4. T. Q. Xie, Z. G. Wang, and Y. T. Pan, "High-speed optical coherence tomography using fiberoptic acousto-optic phase modulation," Opt. Express **11**, 3210 (2003).
5. K. K. M. B. D. Silva, A. V. Zvyagin, and D. D. Sampson, "Extended range, rapid scanning optical delay line for biomedical interferometric imaging," Electron. Lett. 35, 1404 (1999).
6. Amy L. Oldenburg, J. Joshua Reynolds, Daniel L. Marks, and Stephen A. Boppart, "Fast-Fourier-Domain Delay Line for *in vivo* Optical Coherence Tomography with a Polygonal Scanner," Appl. Opt. **42**, 4606-4611 (2003).
7. D. Yelin, S. H. Yun, B. E. Bouma, and G. J. Tearney, "Three-dimensional imaging using spectral encoding heterodyne interferometry," Opt. Lett. 30, 1794-1796 (2005).
8. Michael Choma, Marinko Sarunic, Changhuei Yang, and Joseph Izatt, "Sensitivity advantage of swept source and Fourier domain optical coherence tomography," Opt. Express **11**, 2183-2189 (2003).
9. R. Leitgeb, C. Hitzenberger, and Adolf Fercher, "Performance of Fourier domain vs. time domain optical coherence tomography," Opt. Express **11**, 889-894 (2003).
10. J. Hogan, C. Wilson, "Multiple reference non-invasive analysis system," U.S. Patent 7,526,329, 2009 April 28.
11. J. Hogan, "Frequency resolved imaging system. ," U.S. Patent 7,751,862, 2010 July 6.
12. R. V. Sorin, D. M. Baney, "A simple intensity noise reduction technique for optical low coherence reflectometry," IEEE Photonics Techn. Lett. 4, 1404 – 1406, (1992).